Earthq Eng & Eng Vib (2023) 22: 1015-1030 **DOI**: https://doi.org/10.1007/s11803-023-2217-5

# Resonance analysis of a high-speed railway bridge using a stochastic finite element method

Xiang Ping[1,2†], Yan Weiran[2‡], Jiang Lizhong[2†], Zhou Wangbao[2†], Wei Biao[2†] and Liu Xiang[3§]

1. *Hunan International Scientific and Technological Innovation Cooperation Base of Advanced Construction and Maintenance Technology of Highway, Changsha University of Science and Technology, Changsha 410114, China*
2. *School of Civil Engineering, Central South University, Changsha 410075, China*
3. *School of Civil Engineering, Fujian University of Technology, Fuzhou 350118, China*

**Abstract:** There is always some randomness in the material properties of a structure due to several circumstances and ignoring it increases the threat of inadequate structural safety reserves. A numerical approach is used in this study to consider the spatial variability of structural parameters. Statistical moments of the train and bridge responses were computed using the point estimation method (PEM), and the material characteristics of the bridge were set as random fields following Gaussian random distribution, which were discretized using Karhunen-Loève expansion (KLE). The following steps were carried out and the results are discussed herein. First, using the stochastic finite element method (SFEM), the mean value and standard deviation of dynamic responses of the train-bridge system (TBS) were examined. The effectiveness and accuracy of the computation were then confirmed by comparing the results to the Monte-Carlo simulation (MCS). Next, the influence of the train running speed, bridge vibration frequency, and span of the bridge on dynamic coefficient and dynamic response characteristics of resonance were discussed by using the SFEM. Finally, the lowest limit value of the vibration frequency of the simple supported bridges (SSB) with spans of 24 m, 32 m, and 40 m are presented.

**Keywords:** train-bridge system; material randomness; Karhunen-Loève expansion; Gauss integral; dynamic coefficient; natural frequency

## 1 Introduction

At present, high-speed railway (HSR) bridges are technologically mature, resulting in better ride comfort, usage of land resources, and lower passenger travel costs. When a train runs through a bridge, the bridge and train will couple together (Montenegro *et al*., 2016, 2021). It is better to regard the train and bridge as a system for calculation. For example, Chen *et al*. (2018) and Chen and Zhai (2019) put forward the analytical method of single pier settlement and continuous multi-ton settlement limit of simply supported bridge on HSR. The upper limit value of the above-mentioned structural deformation was proposed by numerical simulation, which provides a convenient method for train running analysis. In the work of Yang and Wu (2002), the behavior of trains running over bridges shaken by earthquakes were discussed. Liu *et al*. (2021a) proposed the safety indexes of a HSR train running on a bridge under an earthquake, which is convenient for engineers to design and use.

For a real structure, due to limitations in the process of making components in the factory and installation errors caused by artificial factors on a construction site, all the parameters of each part of the structure have a certain randomness, and there is an unavoidable deviation compared with the design value under the ideal state. In addition to the stochastic track irregularity (Lai *et al*., 2021), the material properties are also random fields, which will affect the dynamic responses of the train bridge station (TBS). In addition, the comfort level and even running reliability of the train will be affected. On the basis of the conclusions of work of Liu *et al*. (2020a), the sensitivity of the bridge dynamic response to the random parameters of the bridge is much greater than that of track irregularity.

More and more focus has been placed on a more thorough numerical model that accounts for the unpredictability of parameter space in the present study

**Correspondence to**: Liu Xiang, School of Civil Engineering, Fujian University of Technology, Fuzhou 350118, China
Tel: +86-18659472582
E-mail: liuxiang@fjut.edu.cn
†Professor; ‡Master Student; §PhD

**Supported by:** Open Fund of Hunan International Scientific and Technological Innovation Cooperation Base of Advanced Construction and Maintenance Technology of Highway (Changsha University of Science and Technology) Project Number kfj210803, National Natural Science Foundation of China under Grant Nos. U1934207 and 11972379, and Fujian University of Technology under Grant No. GY-Z21181
**Received** December 18, 2021; **Accepted** March 4, 2023

on numerical simulation of dynamic properties of the TBS. For example, Sofi and Romeo (2018) analyzed the uncertainty structure from two different perspectives of probability and non-probability, and compared the response variability of different random models. Jin *et al*. (2015, 2020) derived the dynamical equation of the TBS on the basis of the principle of virtual work, and analyzed the lateral random response of the system by using the pseudo excitation method. Perrin *et al*. (2013) proposed a method to generate more accurate track geometry by combining experimental measurement and numerical simulation. Xu *et al*. (2017, 2018, 2020) researched the dynamic response of the TBS using the probability density evolution method, and proposed a hybrid method to resolve the problem of the variation of the dominant frequency of the TBS and its subsystems, which can simultaneously realize the fine step and the coarse step. The calculation results are compared with Monte-Carlo simulation (MCS) to verify the accuracy. Based on the first-order shear deformation theory, Chang (2014) carried out the stochastic analysis of a simply supported laminated composite bridge with random parameters, and studied the influence of different vehicle speed and load driving frequency on the deflection of the laminated composite bridge. Çavdar *et al*. (2010) proposed a stochastic finite element method (SFEM) for cable-stayed bridges under seismic action considering the stochastic process of elasticity and density of material properties. Xin *et al*. (2019) modelled a train-ballasted track-bridge system, and considered the randomness of geometric parameters, system damping and track irregularity, and analyzed the sensitivity of the system response to the different factors. The method called Karhunen-Loève expansion-point estimation method (KLE-PEM) was applied to calculate a TBS model considering the randomness of track irregularity, and obtained the mean value and standard deviation (Std.D) of the dynamic model (Jiang *et al*., 2019; Liu *et al*., 2020a, 2020b, 2021a, 2021b).

When a train passes across the HSR bridge, it may be thought of as an excitation source operating on the bridge′s structure. The resonance phenomenon will manifest in the TBS when the bridge′s inherent frequency is near to the train′s excitation frequency (Yang *et al*., 2019, 1997; Yang and Yau, 2015, 2017; Zeng *et al*., 2016; Gharad and Sonparote, 2021). Consequently, it is of great practical value to study the limit value of various system parameters of HSR bridges and their influence on the dynamic characteristics of the TBS. Considering several kinds of factors, Xin *et al*. (2020) introduced stochastic analysis into the study of resonance characteristics of TBS, and expounded the statistical characteristics of stochastic resonance. Siringoringo and Fujino (2012) estimated the bridge′s natural frequency by using the acceleration response of the train using finite element (FE) simulation and compared it with the measured data of a full-scale short span simple supported bridges (SSB).

The above literature describes a series of studies that have been conducted on a random TBS system and bridge resonance. According to Jiang *et al*. (2019), the variability of bridge parameters has a significant impact on the natural vibration characteristics of the bridge, which will further affect the resonance speed of railway bridges, and the material parameters of the bridge are a random field. Based on this, the resonance effect of TBS is analyzed herein considering the random field of material properties.

To fully study the resonance phenomenon of bridges considering material random fields, a dynamic SFEM model of TBS was established, in which the material properties such as modulus of elasticity and density were set as random processes following Gaussian random distribution, and the KLE was used to discretize them. The PEM was used to calculate the statistical moments of responses. The calculation accuracy of the dynamic TBS model was compared with the field test data, and the statistical moments of structural responses were compared with those obtained by the MCS. Then, the displacement and acceleration responses of the TBS under different conditions were further analyzed. Based on this random analysis method, the recommended limit values of vertical natural frequencies of a bridge with different spans are proposed.

## 2 Stochastic finite element method

### 2.1 Karhunen-Loève expansion (KLE)

The KLE is an orthogonal series expansion technique that works well with second moment random fields. KLE can expand the random field into a cosine function and into the sum of a number of deterministic continuous functions and random variables when the uncertainty of the system follows a Gaussian random distribution (Ghanem and Spanos, 2003). Let the mean of the stochastic field $\omega(x)$ be $\overline{\omega}(x)$, then $\omega(x)$ can be expressed by Eq. (1).

$$\omega(x)=\overline{\omega}(x)+\tilde{\omega}(x) \tag{1}$$

where $\omega(x)$ is a stochastic process with the mean value of $\overline{\omega}(x)$. The function of vector $x$ is defined in the field $\Omega$, where $\theta$ belongs to the random event space $D$. If the covariance function of $\tilde{\omega}(x)$ is $C_{\omega}(x_1, x_2)$, it must be a bounded, symmetric and nonnegative definite function according to the properties of the covariance function, and it can be expressed as the following formula,

$$C_{\omega}(x_1,x_2)=\sum_{k=1}^{\infty}\lambda_k\varphi_k(x_1)\varphi_k(x_2) \tag{2}$$

where $\lambda_k$ is the eigenvalue of covariance function and $\varphi_k(x)$ is the eigenfunction. Equation (2) can be solved by the following equation,

$$\int_{\Omega} C_{\omega}(x_1, x_2)\varphi_k(x_1)\mathrm{d}x_1 = \lambda_k \varphi_k(x_2) \tag{3}$$

Equation (3) can be solved by the Fredholm integral, and it can be expressed as the following equation,

$$\int_{\Omega} \varphi_k(x_1)\varphi_k(x_2)\mathrm{d}x = \delta_{kl} \tag{4}$$

where $\delta_{kl}$ is a Kronecker delta function.

Therefore, the $\tilde{\omega}(x)$ can be transformed into a linear combination of $\varphi_k(x)$ and the independent random variable system $\xi_k(\theta)$, which can be written as,

$$\tilde{\omega}(x,\theta)=\sum_{k=0}^{\infty}\xi_k(\theta)\sqrt{\lambda_k}\varphi_k(x) \tag{5}$$

where $\xi_k(\theta)$ ($k$=1, 2, …) is the uncorrelated random variable, and $E(\xi_k(\theta))$=0,

Thus, $\omega(x)$ can be expressed as:

$$\omega(x,\theta) = \bar{\omega}(x) + \sum_{k=0}^{\infty}\xi_k(\theta)\sqrt{\lambda_k}\varphi_k(x) \tag{6}$$

Usually, a finite dimension can be used to obtain the random field within the permitted error range, and it can be expressed as,

$$\omega(x,\theta) \approx \bar{\omega}(x) + \sum_{k=0}^{M}\xi_k(\theta)\sqrt{\lambda_k}\varphi_k(x) \tag{7}$$

where $M$ is the number of truncated items.

### 2.2 Point estimation method (PEM)

The random field discussed in this study obeys Gaussian random distribution, so the variables in the expression of the KLE obey the standard normal distribution. Assuming that $Y$=$h(x)$ is a continuous random variable and $p(x)$ is its probability density function, its expectation and variance can then be obtained by the following formula:

$$E[Y] = E[h(x)] = \int_{-\infty}^{\infty} h(x)\,p(x)\mathrm{d}x \tag{8}$$

$$M_{z2} = D[Y] = E\left[(Y-\mu)^2\right] = \int_{-\infty}^{\infty}[h(x)-\mu]^2\,p(x)\mathrm{d}x \tag{9}$$

where $x$ is the variable value; $E$ is the math expectation and $D$ is the variance; and $\mu = E[Y]$. $M_{z2}$ denotes the second central moment.

There are many random variables in the expansion of the stochastic process, which can be simplified by the dimension reduction method. $h(x)$ can be transformed into a combination of one-dimensional variables $h^1(X)$ according to Rahman and Xu (2004):

$$h(x) \cong h^1(x) = \sum_{i=1}^{n} h_i(x_i) - (n-1)h(c) \tag{10}$$

where $n$ is the number of random variables; $c$ denotes the reference value, and $h(c)$ represents the corresponding response value when all variables are reference values.

Substituting Eq. (10) to Eqs. (8) and (9), the following equations can be obtained (Zhao and Ono, 2000),

$$E[Y] \cong \sum_{i=1}^{n} E[h_i(X_i)] - (n-1)h(c) \tag{11}$$

$$M_{z2} = D[Y] \cong \sum_{i=1}^{n} E\left\{\left[h_i(X_i)-\mu\right]^2\right\} - (n-1)[h(c)-\mu]^2 \tag{12}$$

where $h_i(X_i)$ denote that all variables except the $i$th variable are references.

According to the above process and Gaussian integral theory, the following formula can be used for further calculation,

$$E[h_i(X_i)] = \sum_{l=1}^{a}\frac{w_{\mathrm{GH},l}}{\sqrt{\pi}}h_i\left(\sqrt{2}x_{\mathrm{GH},l}\right) \tag{13}$$

$$E\left[\left(h_i(X_i)-\mu\right)^2\right] = \sum_{l=1}^{a}\frac{w_{\mathrm{GH},l}}{\sqrt{\pi}}\left[h_i\left(\sqrt{2}x_{\mathrm{GH},l}\right)-\mu\right]^2 \tag{14}$$

where $a$ is the number of Gaussian-Hermite integral points. $x_{\mathrm{GH}}$ is the abscissa of the quadrature points, and $w_{\mathrm{GH}}$ is the weight coefficient corresponding to $x_{\mathrm{GH}}$. When the number of Gaussian integral points are three, five and seven, the corresponding parameters are shown in Table 1, Table 2 and Table 3. In general, the reference value $c$ can be set to zero.

**Table 1 Abscissa and weight coefficient of three points Gauss integral**

| Integral point | 1 | 2 | 3 |
|---|---|---|---|
| $x_{\mathrm{GH}}$ | –1.22474 | 0 | 1.22474 |
| $w_{\mathrm{GH}}$ | 0.29541 | 1.18164 | 0.29541 |

**Table 2 Abscissa and weight coefficient of five points Gauss integral**

| Integral point | 1 | 2 | 3 | 4 | 5 |
|---|---|---|---|---|---|
| $x_{\mathrm{GH}}$ | –2.02018 | –0.958572 | 0 | 0.958572 | 2.02018 |
| $w_{\mathrm{GH}}$ | 0.0199532 | 0.393619 | 0.945309 | 0.393619 | 0.0199532 |

**Table 3 Abscissa and weight coefficient of seven points Gauss integral**

| Integral point | 1 | 2 | 3 | 4 | 5 | 6 | 7 |
|---|---|---|---|---|---|---|---|
| $x_{GH}$ | 2.65196 | 1.67355 | –0.81629 | 0 | 0.81629 | 1.67355 | 2.65196 |
| $w_{GH}$ | $9.71781\times10^{-4}$ | $5.45456\times10^{-2}$ | 0.425607 | 0.810265 | 0.425607 | $5.45456\times10^{-2}$ | $9.71781\times10^{-4}$ |

### 2.3 Dynamic SFEM based on KLE-PEM

In engineering structures, due to some engineering deviations, materials exhibit random field characteristics. In this study, the modulus of elasticity $E_b$ and density $\rho_b$ of the bridge structure are supposed to obey Gaussian random distribution (Wu and Law, 2010). Taking the SFEM of elastic modulus $E_b$ for example, according to the above theory, the randomness of $E_b$ can be expressed with KLE, and it can be written as

$$E_b(x,\theta)=\overline{E}_b(x)+\tilde{E}_b(x) \tag{15}$$

with

$$\tilde{E}_b(x,\theta)=\sum_{i=1}^{M_E}\xi_i(\theta)\sqrt{\lambda_i}\varphi_i(x) \tag{16}$$

where $\overline{E}_b(x)$ is the mean of modulus of elasticity and $\tilde{E}_b(x)$ is the random part of elastic modulus; $M_E$ is the number of truncated terms of the random expansion; and $\boldsymbol{\xi}_i$ is a combination of standard random variables.

According to the FE theory, the stiffness matrix of the structural element can be expressed as

$$\boldsymbol{K}^e=\int_l \boldsymbol{B}_e^T E_b(x,\theta)\boldsymbol{I}\boldsymbol{B}_e\mathrm{d}x=\overline{\boldsymbol{K}}^e+\tilde{\boldsymbol{K}}^e \tag{17}$$

with

$$\overline{\boldsymbol{K}}^e=\int_l \boldsymbol{B}_e^T \overline{E}_b(x)\boldsymbol{I}\boldsymbol{B}_e\mathrm{d}x \tag{18}$$

$$\tilde{\boldsymbol{K}}^e=\int_l \boldsymbol{B}_e^T \tilde{E}_b(x,\theta)\boldsymbol{I}\boldsymbol{B}_e\mathrm{d}x=\sum_{i=1}^{M_E}\xi_i\tilde{\boldsymbol{K}}_i^e \tag{19}$$

$$\tilde{\boldsymbol{K}}_i^e=\int_l \boldsymbol{B}_e^T\sqrt{\lambda_i}\varphi_i(x)\boldsymbol{I}\boldsymbol{B}_e\mathrm{d}x \tag{20}$$

where $\boldsymbol{B}_e=\dfrac{\mathrm{d}^2\boldsymbol{N}_e}{\mathrm{d}x^2}$, and $\boldsymbol{N}_e$ is the shape function matrix (Liu *et al*., 2022).

Similarly, the structural mass matrix of the element considering the material random field can be obtained, which can be written as the following equations,

$$\boldsymbol{M}^e=\overline{\boldsymbol{M}}^e+\tilde{\boldsymbol{M}}^e \tag{21}$$

with

$$\overline{\boldsymbol{M}}^e=\int_l \boldsymbol{N}_e^T\overline{\rho}(x)A\boldsymbol{N}_e\mathrm{d}x \tag{22}$$

$$\tilde{\boldsymbol{M}}^e=\int_l \boldsymbol{N}_e^T\tilde{\rho}(x)A\boldsymbol{N}_e\mathrm{d}x=\sum_{i=1}^{M_\rho}\xi_i\tilde{\boldsymbol{M}}_i^e \tag{23}$$

$$\tilde{\boldsymbol{M}}_i^e=\int_l \boldsymbol{N}_e^T\sqrt{\lambda_i}\varphi_i(x)A\boldsymbol{N}_e\mathrm{d}x \tag{24}$$

where $\overline{\rho}(x)$ and $\tilde{\rho}(x)$ represent the mean part and random part in the density random field, respectively; and $A$ denotes the area of the section.

After obtaining the global stiffness and mass matrices, the dynamic equation of the bridge can be expressed as the following formula,

$$\boldsymbol{M}\ddot{\boldsymbol{X}}(r,\theta)+\boldsymbol{C}\dot{\boldsymbol{X}}(r,\theta)+\boldsymbol{K}\boldsymbol{X}(r,\theta)=\boldsymbol{F}(r,\theta) \tag{25}$$

where $\boldsymbol{F}(r,\theta)$ denotes the force vector; and $\boldsymbol{C}$ denotes the damping matrix, which is assumed as the Rayleigh damping and can be expressed as,

$$\boldsymbol{C}=\alpha\boldsymbol{M}+\beta\boldsymbol{K} \tag{26}$$

where $\alpha$=0.25 and $\beta$=0.5.

According to Eqs. (11) to (14), the values corresponding to each random variable can be brought into Eq. (25) one by one to obtain the response of interest, such as the midspan displacement response $R_i^l(t)$, and then all $R_i^l(t)$ can be summarized for calculation to obtain the statistics of SFEM system response. Note that when zero is chosen as the reference point value $c$, except for the $i$-th $\xi_i$, all other $\xi_i$ are equal to zero, which means that Eqs. (17) and (21) can be transformed as,

$$\begin{cases}\boldsymbol{K}^e=\overline{\boldsymbol{K}}^e+\xi_i\tilde{\boldsymbol{K}}^e\\ \boldsymbol{M}^e=\overline{\boldsymbol{M}}^e\end{cases} \tag{27}$$

or

$$\begin{cases}\boldsymbol{K}^e=\overline{\boldsymbol{K}}^e\\ \boldsymbol{M}^e=\overline{\boldsymbol{M}}^e+\xi_i\tilde{\boldsymbol{M}}^e\end{cases} \tag{28}$$

The detailed process is shown in Fig. 1. It can be seen that when the elastic modulus and density are independent, the calculation times $N_c$ of the dynamic model that SFEM needs to call is

$$N_c=N_r(a-1)+1 \tag{29}$$

where $N_r$ denote the total number of random variables; that is, the total number of truncated items.

## 3 Train-bridge model

### 3.1 Model establishment

As shown in Fig. 2, taking the SSB as an example, when the train passes over the bridge, the train, track and bridge will have corresponding responses that then affect the running state of the whole system. In general, there are various uncertain factors in the TBS. In the research of Liu *et al*. (2020), the responses of SSB considering track irregularity and structural parameters were analyzed, and the results showed that when the research object is the bridge, the randomness of track irregularity can be ignored, and only using deterministic irregularity samples can obtain accurate enough results. The research objects of the cases were mainly the bridge structure, so only the random parameters of the bridge structure are considered.

The TBS model is shown in Fig. 3. Based on the principle of conservation of potential energy in a dynamic system, the motion equation of the TBS can be derived as:

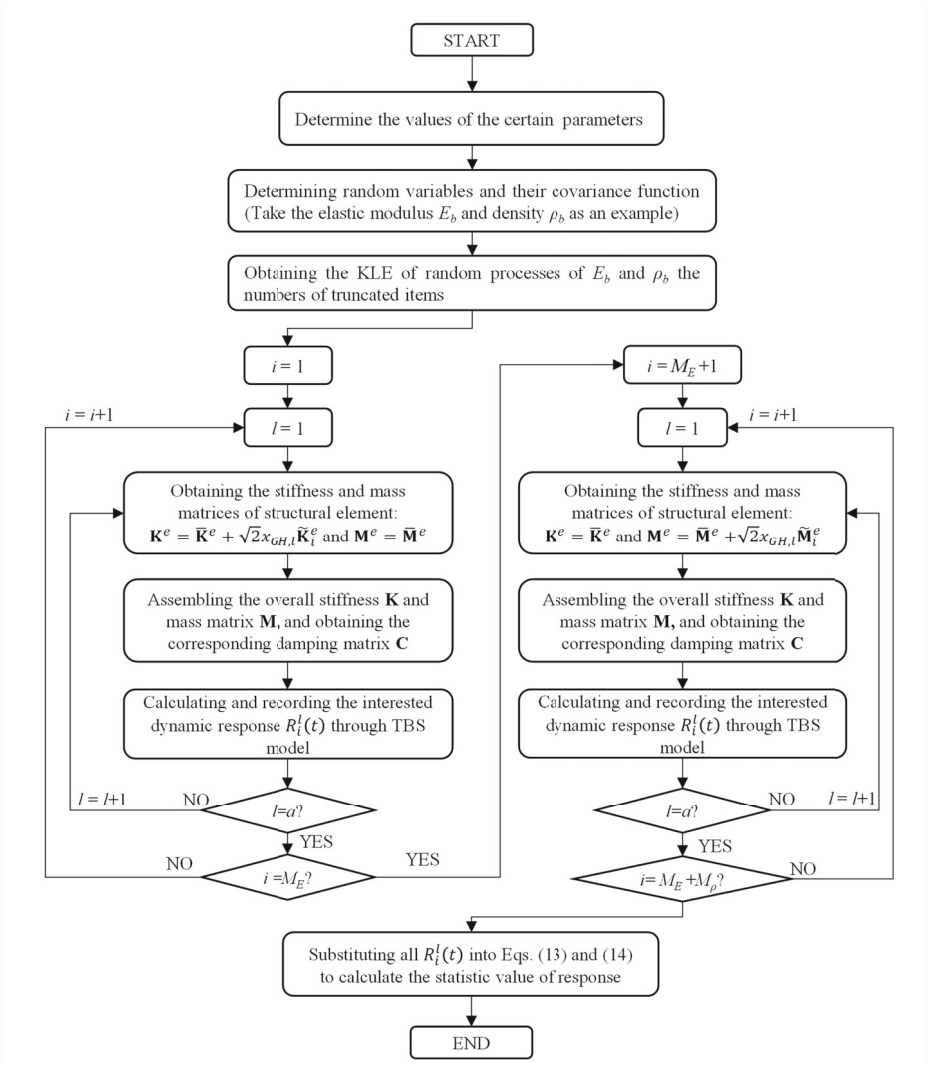


**Fig. 1 Flowchart of SFEM for calculating TBS**

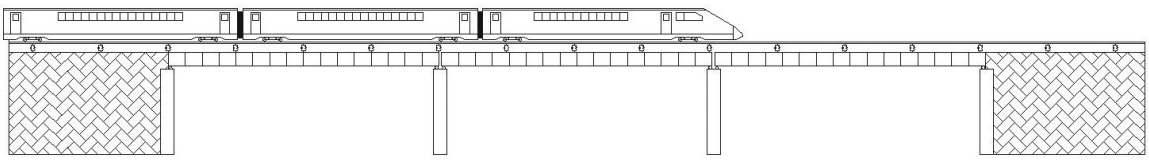

**Fig. 2 Train passing through simply supported bridge**

$$\begin{bmatrix} \boldsymbol{M}_{\mathrm{tt}} & & \\ & \boldsymbol{M}'_{\mathrm{rr}} & \\ & & \mathbf{M}_{\mathrm{bb}} \end{bmatrix} \begin{Bmatrix} \ddot{\boldsymbol{X}}_{\mathrm{t}} \\ \ddot{\boldsymbol{X}}_{\mathrm{r}} \\ \ddot{\boldsymbol{X}}_{\mathrm{b}} \end{Bmatrix} + \begin{bmatrix} \boldsymbol{C}_{\mathrm{tt}} & \boldsymbol{C}_{\mathrm{tr}} & \\ \boldsymbol{C}_{\mathrm{rt}} & \boldsymbol{C}_{\mathrm{rr}} & \\ & & \mathbf{C}_{\mathrm{bb}} \end{bmatrix} \begin{Bmatrix} \dot{\boldsymbol{X}}_{\mathrm{t}} \\ \dot{\boldsymbol{X}}_{\mathrm{r}} \\ \dot{\boldsymbol{X}}_{\mathrm{b}} \end{Bmatrix} + \begin{bmatrix} \boldsymbol{K}_{\mathrm{tt}} & \boldsymbol{K}_{\mathrm{tr}} & \\ \boldsymbol{K}_{\mathrm{tr}} & \boldsymbol{K}_{\mathrm{rr}} & \\ & & \boldsymbol{K}_{\mathrm{bb}} \end{bmatrix} \begin{Bmatrix} \boldsymbol{X}_{\mathrm{t}} \\ \boldsymbol{X}_{\mathrm{r}} \\ \boldsymbol{X}_{\mathrm{b}} \end{Bmatrix} = \begin{Bmatrix} \boldsymbol{F}_{\mathrm{t}} \\ \boldsymbol{F}_{\mathrm{r}} \\ \boldsymbol{F}_{\mathrm{b}} \end{Bmatrix} \tag{30}$$

where $\boldsymbol{M}$, $\boldsymbol{C}$ and $\boldsymbol{K}$ denote mass, damping and stiffness matrices, respectively; the subscripts tt, rr and bb denote the train, track and bridge; the subscripts tr and rt denote the coupled part of train and rail; $\ddot{\boldsymbol{X}}$, $\dot{\boldsymbol{X}}$ and $\boldsymbol{X}$ denote acceleration, velocity and displacement vectors, respectively; and the subscripts t, r and b denote train, rail and bridge, respectively. $\boldsymbol{F}$ denotes the force vectors; among them, $\boldsymbol{F}_{\mathrm{t}}$ includes the dead weight of the train and the wheel rail interaction force. In the model, the wheel rail is always closely attached, and the wheel rail interaction force is the excitation of track irregularity, which is calculated by using a linear model. Taking one wheel set as an example, the wheel rail force at time of $t$ can be calculated by the following formula,

$$F(t) = k_{\mathrm{p}} u(t) + c_{\mathrm{p}} u'(t) + m_{\mathrm{w}} u''(t) \tag{31}$$

where $k_{\mathrm{p}}$ and $c_{\mathrm{p}}$ denote stiffness and damping value of primary suspension, respectively; $m_{\mathrm{w}}$ denotes the mass of wheelset; and $u(t)$, $u'(t)$ and $u''(t)$ are the irregularity, first order derivation of track irregularity, and second order derivation of track irregularity acting on the wheel set at time $t$, respectively. More detailed information can be found in Liu *et al.* (2020b).

### 3.2 Model verification

Track irregularity samples were generated by German low interference track spectrum. The numerical simulation results of the SSB were compared with the field measured data for validation. The measuring instrument was the image by interferometric survey-frequency structures (IBIS-FS) and the measured bridge was the Zhuzhou Xiangjiang bridge on the Wuhan Guangzhou passenger dedicated line. The IBIS-FS can monitor the static and dynamic deflection of the bridge. The components of the IBIS-FS include a PC as the user interface, a radar head with two antennas (receiving signals) and a tripod, as shown in Fig. 4. The IBIS-FS radar points to the bottom surface area of the measurement position on the bridge deck, and the equipment measures the displacement of the target point illuminated by the electromagnetic beam emitted by the antenna. The device will measure the displacement in the viewing direction in all range bins located in the irradiation area. Then the vertical dynamic deformation can be obtained through the corresponding angle relationship. The measured section was a SSB with the span of 32 m. The train had sixteen carriages, and the mid-span displacement of the bridge was tested. The comparison results are shown in Fig. 5.

It can be seen that the three groups of test results are very close to the numerical calculation results. Since the train model was composed of sixteen carriages, there were 15 peaks in the dynamic response curves. The average values of three groups of test results at each of five peaks are shown in Table 4, where $\eta$ is the ratio of the numerical result to the measured average result and the time column shows the time corresponding to the peak displacement. The three groups of test data are

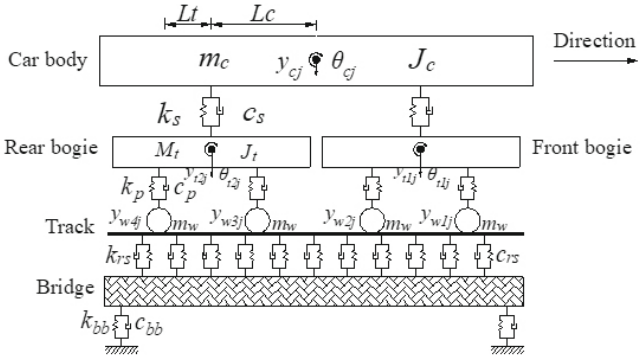


**Fig. 3 TBS model**

**Fig. 4 Survey site**

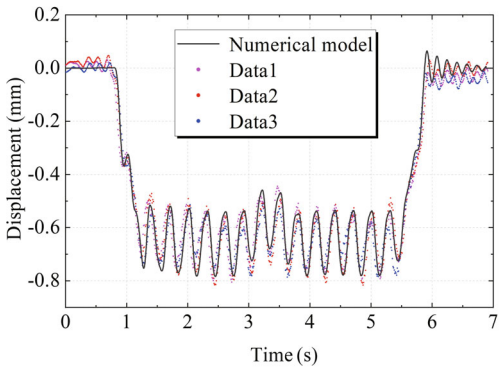


**Fig. 5 Comparison of bridge mid-span displacement time history curves**

discrete, and because the TBS itself is a random system, the load of each train is different, and the TBS is excited by random track irregularity. The ratio of the calculated results to the average measured data is in the range of 0.95–1.13, which indicates that the numerical model has a very high accuracy. The variation trend of the bridge mid-span displacement time history curve is completely consistent with the measured data.

### 3.3 Calculation efficiency and accuracy

An instance of a HSR train passing through a 32 m standard SSB was examined to examine the effectiveness and accuracy of KLE-PEM in the calculation of the TBS model while taking the spatial random field of the material properties into consideration. The German ICE3 HSR train was adopted, and the parameters are shown in Table 5, and the train speed was 300 km/h. The bridge had a single span of 32 m and was simply supported. The track slab gave mass and stiffness to the bridge. Other specific values are presented in Table 6.

In railway bridge dynamics, there are many random variables, such as concrete elastic modulus, concrete density, ballast density weight, dimensions of the member, and so on (Rocha *et al*., 2012, 2016). At present, China′s HSR bridges are basically prefabricated components, and their dimensional variability is almost negligible. In addition, according to the relevant research results (Jiang *et al*., 2019; Liu *et al*., 2020a) for the materials of the bridge, the dynamic characteristics of the TBS is most sensitive to the randomness of the elastic modulus and density. Therefore, in this numerical calculation, the modulus of elasticity $E_b$ and density $\rho_b$ are set to obey Gaussian random fields, and the coefficients of variation are 0.06 and 0.04, respectively (Liu *et al*., 2020a). The covariance function of the Gaussian random field is (Wu and Law, 2010):

$$C(x_1, x_2) = \sigma^2 \mathrm{e}^{-(|x_1 - x_2|/l_\mathrm{a})} \tag{32}$$

where $l_\mathrm{a}$ denotes the correlation length, and is equal to 5.

The number of truncation terms was ten. Considering there were two kinds of random fields, there were twenty independent random variables in the system. The random system responses with three, five and seven integration points were calculated, and named as KLE-PEM-3, KLE-PEM-5 and KLE-PEM-7, respectively. The random responses of the system obtained from the MCS with 20,000 calculations were regarded as the exact solution to validate the result of KLE-PEM, and the results are shown in Fig. 6 and Fig. 7. The relative error $R_\mathrm{E}$ was adopted to evaluate the precision of KLE-PEM, which can be expressed as

$$R_\mathrm{E} = \left| \frac{R_\mathrm{KLE\text{-}PEM} - R_\mathrm{MCS}}{R_\mathrm{MCS}} \right| \times 100\% \tag{33}$$

where $R_\mathrm{KLE\text{-}PEM}$ is the result of KLE-PEM, $R_\mathrm{MCS}$ is the result of MCS.

**Table 4 Peak value of midspan displacement obtained from numerical and test**

| Time (s) | Numerical result (mm) | Test 1 (mm) | Test 2 (mm) | Test 3 (mm) | Average (mm) | $\eta$ |
|---|---|---|---|---|---|---|
| 1.84 | –0.770 | –0.710 | –0.762 | –0.746 | –0.739 | 1.04 |
| 2.75 | –0.781 | –0.752 | –0.794 | –0.752 | –0.766 | 1.02 |
| 3.65 | –0.737 | –0.721 | –0.759 | –0.771 | –0.751 | 0.98 |
| 4.54 | –0.778 | –0.759 | –0.769 | –0.696 | –0.741 | 1.05 |
| 5.44 | –0.724 | –0.718 | –0.702 | –0.765 | –0.728 | 0.99 |

**Table 5 Parameters of ICE3 model**

| Parameters | Symbol | Unit | Motor car | Trail car |
|---|---|---|---|---|
| Car body mass | $m_\mathrm{c}$ | kg | $4.56\times10^4$ | $4.9\times10^4$ |
| Bogie mass | $m_\mathrm{t}$ | kg | $4.4\times10^3$ | $2.7\times10^3$ |
| Wheel mass | $m_\mathrm{w}$ | kg | $2.4\times10^3$ | $2.4\times10^3$ |
| Moment of inertia of car body | $J_\mathrm{c}$ | kg·m$^2$ | $2.397\times10^6$ | $2.576\times10^6$ |
| Bogie moment of inertia | $J_\mathrm{t}$ | kg·m$^2$ | $5.42\times10^3$ | $3.33\times10^3$ |
| Half wheelbase | $L_\mathrm{t}$ | m | 1.25 | 1.25 |
| Bogie half distance | $L_\mathrm{c}$ | m | 8.69 | 8.69 |
| Primary suspension stiffness | $k_\mathrm{p}$ | N/m | $1.124\times10^6$ | $6.9\times10^5$ |
| Secondary suspension stiffness | $k_\mathrm{s}$ | N/m | $5.61\times10^5$ | $6.03\times10^5$ |
| Primary suspension damping | $c_\mathrm{p}$ | N·s/m | $8.8\times10^3$ | $5.4\times10^3$ |
| Secondary suspension damping | $c_\mathrm{s}$ | N·s/m | $2.7\times10^4$ | $2.9\times10^4$ |

According to Fig. 6(a), when the train with eight carriages passed the bridge, there were seven wave peaks in the mean value (mean) response process. The average relative error analysis of the midspan displacement response from 1.5 s to 3.5 s shows that the average relative error of MCS and KLE-PEM-3, KLE-PEM-5, KLE-PEM-7 is 0.015%, 0.015% and 0.017%, respectively. Figure 6(b) gives the standard deviation value (Std.D) of the bridge displacement. The calculated results of MCS are slightly higher than those of KLE-PEM at the curve peaks, and the average errors from 1.5 s to 3.5 s are 1.259%, 1.258% and 1.257%, respectively. The calculated data of the two methods are very similar.

Figure 7(a) shows the mean value of the time history curve of a car body acceleration. The average relative errors of the two calculation methods in 1.5 s to 3.5 s are 0.339%, 0.339% and 0.466%, respectively. Figure 7(b) indicates that the Std.D of the car body acceleration increases when the train enters the bridge until it reaches

**Table 6 Parameters of rail and bridge**

| Parameters | Symbol | Unit | Value |
|---|---|---|---|
| Rail section area | $A_r$ | $m^2$ | $7.6\times10^{-3}$ |
| Moment of inertia of rail section | $I_r$ | $m^4$ | $2\times3.22\times10^{-5}$ |
| Elastic modulus of rail | $E_r$ | $N/m^2$ | $2.06\times10^{11}$ |
| Rail density | $D_r$ | $kg/m^3$ | $7.85\times10^3$ |
| Cross section area of bridge | $A_b$ | $m^2$ | 7.32 |
| Moment of inertia of bridge section | $I_b$ | $m^4$ | 12.74 |
| Elastic modulus of bridge | $E_b$ | $N/m^2$ | $3.45\times10^{10}$ |
| Bridge density | $D_b$ | $kg/m^3$ | $2.5\times10^3$ |
| Damping ratio | $\zeta$ | - | 0.02 |
| Vertical stiffness of bridge bearing | $k_{bb}$ | N/m | $6.3\times10^{12}$ |
| Vertical damping of bridge support | $C_{bb}$ | N·s/m | $2.04\times10^5$ |
| First natural frequency | $\omega_1$ | Hz | 7.5301 |
| Second natural frequency | $\omega_2$ | Hz | 30.04 |

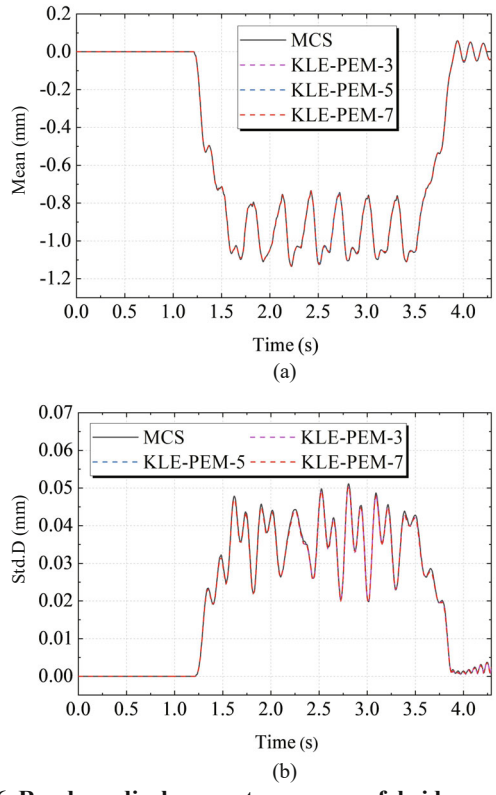


**Fig. 6 Random displacement response of bridge midspan: (a) mean; (b) Std.D**

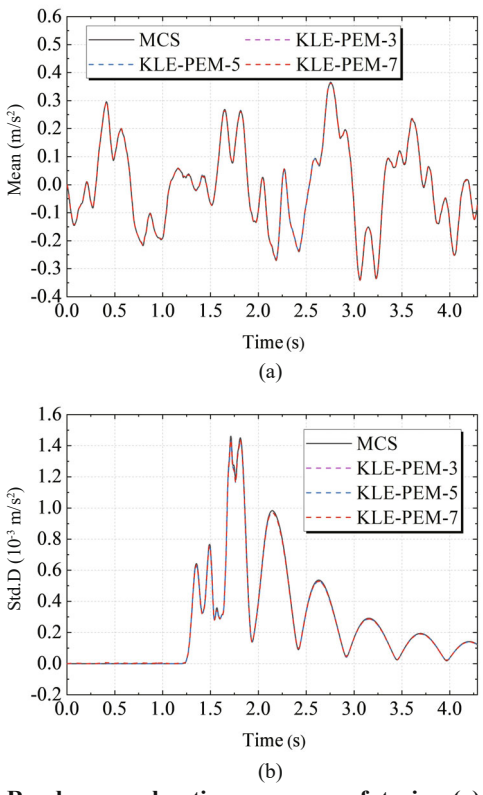


**Fig. 7 Random acceleration response of train: (a) mean; (b) Std.D**

the peak value of $1.440 \times 10^{-6}$ m/s$^2$ in 1.712 s. The average relative errors of the two methods in 1.5 s to 3.5 s are 1.227%, 1.224% and 1.203%, respectively.

According to the above results, the number of Gaussian integration points has little effect on the calculation accuracy, and the calculation results of MCS and KLE-PEM are very similar. To analyze the accuracy of the calculation method more intuitively, the errors of KLE-PEM-3, KLE-PEM-5 and KLE-PEM-7 at the times of 1.7 s and 2.2 s are shown in Table 7 and Table 8. It can be seen that KLE-PEM has a very high accuracy with three Gaussian integral points. On the same computer with 16 G memory and 3.0 GHz dominant frequency, the calculation time of the conventional MCS method with 20,000 calculations was about 16.8 hours; for the KLE-PEM, when the number of Gaussian integration points were three, five and seven, the calculation time was 62 s, 116 s and 172 s, respectively, which is much faster than the traditional MCS method. In the subsequent analysis, three integral points were used for calculation.

### 3.4 Responses of TBS at various speeds

According to the rule of three-times-standard deviation value, the probability of datum distribution in the range of [$\mu$-3$\sigma$, $\mu$+3$\sigma$] is 99.74%, where $\mu$ and $\sigma$ denote mean value and standard deviation value, respectively, and in the range of [$\mu$-3$\sigma$, $\mu$+3$\sigma$], the probability of random events is 99.74%, which can be approximately considered to cover all possible situations. In the subsequent analysis, the maximum of absolute values of $\mu - 3\sigma$ and $\mu + 3\sigma$ is regarded as the maximum probability value.

According to Fig. 8, the results of dynamic response considering the uncertainty of bridge material properties are evidently larger than those of deterministic results, and the change patterns of the curves of the two calculation results are basically the same. Without taking into account the random influence of the material properties, the results indicate that the vertical acceleration distribution of the bridge is 0.24 m/s$^2$ to 2.03 m/s$^2$ and the vertical displacement is 1.04 mm to 1.63 mm; however, when considering the randomness of material properties, the results indicate that the vertical acceleration distribution is 0.26 m/s$^2$ to 2.27 m/s$^2$ and the vertical displacement is 1.16 mm to 1.84 mm; both are larger than those of the deterministic model.

The expansion coefficient $\alpha$ is used to express the increase range of the calculation results of the system dynamic response after considering parameter uncertainty, and the calculation formula is as follows

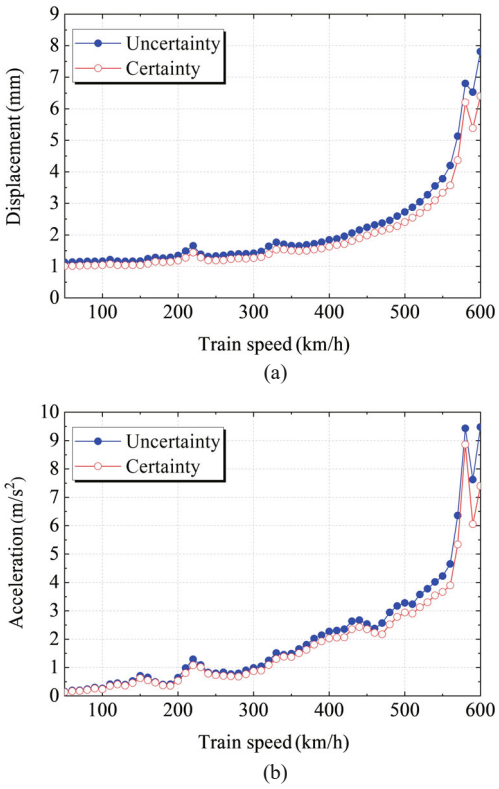


**Fig. 8 Probability maximum and deterministic maximum response of bridge midspan at various speeds: (a) displacement; (b) acceleration**

**Table 7 Relative error at 1.7 s**

| Method | MCS | KLE-PEM-3 | Relative error |
|---|---|---|---|
| Mean of bridge displacement (mm) | –1.0977 | –1.0979 | 0.02% |
| Std.D of bridge displacement (mm) | 0.0372 | 0.0369 | 0.81% |
| Mean of train acceleration (m/s$^2$) | 0.1260 | 0.1260 | 0 |
| StD.d of train acceleration (m/s$^2$) | 1.362 | 1.344 | 1.32% |

**Table 8 Relative error at 2.2 s**

| Method | MCS | KLE-PEM-3 | Relative error |
|---|---|---|---|
| Mean of bridge displacement (mm) | –1.0994 | –1.0995 | 0.01% |
| Std.D of bridge displacement (mm) | 0.0407 | 0.0399 | 1.96% |
| Mean of train acceleration (m/s$^2$) | –0.2452 | –0.2452 | 0 |
| Std.D of train acceleration (m/s$^2$) | 0.9273 | 0.9158 | 1.24% |

to show how the structural dynamic response changes after taking the influence of parameter randomness into account,

$$\alpha = \left| \frac{R_u - R_c}{R_c} \right| \times 100\% \tag{34}$$

where $R_c$ represents the maximum value of the time history response of the system ignoring randomness, and $R_u$ denotes the maximum value of the time history response of the maximum probability value.

Compared with the deterministic results, the average expansion coefficients of the two response uncertainties are 13.05% and 12.51% in this speed range.

The probability maximum and deterministic maximum response of the car body acceleration at different speeds are shown in Fig. 9. The calculation distribution range of the two calculation results is 0.18 m/s$^2$ to 0.40 m/s$^2$ for train speeds between 100 km/h and 400 km/h. The maximum expansion coefficient of the car body acceleration is 0.23 percent, which is much smaller than that of the bridge. It shows that the sensitivity of the bridge response to material randomness is much greater than the sensitivity of the train response to material randomness.

## 4 Resonance analysis based on KLE-PEM

### 4.1 Dynamic coefficient index

A measure known as the dynamic coefficient is used to define the proportionate relationship between a structure's maximal dynamic reaction and its static response. The definition of a dynamic coefficient index $\beta$ for railway bridges supporting train loads is as follows:

$$\beta = \frac{\delta_d}{\delta_s} \tag{35}$$

where $\delta_d$ is the maximum response of midspan displacement caused by train load moving on the bridge; and $\delta_s$ is the maximum response of the midspan displacement due to the static train load.

The dynamic coefficient is related to the bridge's natural frequency and the train's excitation frequency, and the excitation frequency of the train depends on the running speed and location arrangement of the wheel sets. At present, the calculation formula of the dynamic coefficient of HSR and an intercity railway bridge in China is as follows:

$$\beta = \frac{1.44}{\sqrt{L_b} - 0.2} + 0.82 \tag{36}$$

where $L_b$ is the span of the SSB.

For China's HSR, the design criterion stipulated in the code is that the bridge dynamic response caused by the train does not exceed the bridge response caused by design load. Therefore, the calculation method of the allowable dynamic coefficient of the HSR bridge can be obtained as follows:

$$\beta_{\text{allowable}} \le \frac{\text{load effect}_{ZK} \cdot \beta}{\text{load effect}_{\text{train}}} \tag{37}$$

where $\beta$ is calculated by Eq. (36).

The allowable dynamic coefficients of simply supported box girders with spans of 24 m, 32 m and 40 m under different loads and train types are shown in Table 9. CRH2 multiple units has been widely used in China, therefore it is selected herein as the train model for dynamic analysis. The parameters of the CRH2 train are shown in Table 10.

### 4.2 Influence of random field of material properties on dynamic coefficient

For short and medium span simply supported bridges, the excitation frequency $f_v$ of the train running at different speeds can be calculated according to Eq. (38):

$$f_v = \frac{v}{3.6 d_v} \tag{38}$$

where $v$ denotes the train speed, and $d_v$ denotes the carriage spacing.

According to Eq. (38), when the carriage spacing is fixed, the excitation frequency of the train to the bridge is only related to the running speed. According to the resonance theory, while the train's exciting frequency is

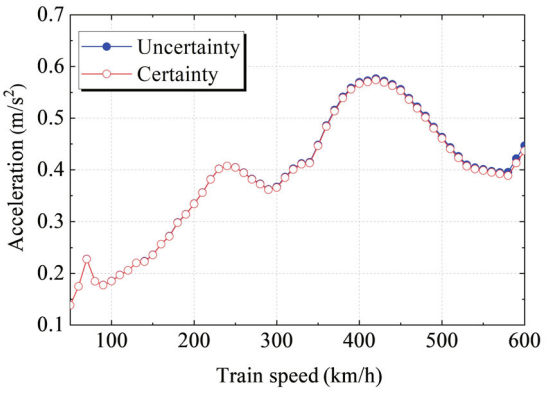


**Fig. 9 Probability maximum and deterministic maximum response of car body acceleration at various speeds**

**Table 9 Allowable dynamic coefficient of different span**

| | ZK load | ICE2 | CRH2 | CRH3 |
|---|---|---|---|---|
| 24 m | 1.13 | 2.69 | 3.26 | 2.68 |
| 32 m | 1.06 | 2.55 | 3.65 | 3.00 |
| 40 m | 1.06 | 2.55 | 3.65 | 3.00 |

equivalent to 1/$n$ ($n$=1, 2, 3, …) of the bridge′s natural frequency, the bridge structure will produce resonance or super-harmonic resonance. When the bridge′s natural frequency is $f_b$, the $n$-order super-harmonic resonance velocity $v_{v,n}$ can be obtained by the following formula (Yang *et al*., 2004),

$$v_{v,n} = \frac{3.6d_v}{n} f_b \tag{39}$$

The dynamic coefficients related to the vertical vibration frequency of various bridges are estimated as the train travels through a 32 m SSB using the CRH2 HSR train as an example. The vertical frequencies of SSB were 5.13 Hz, 6.00 Hz, and 7.51 Hz, respectively, which were the natural frequencies commonly used in railway bridges. Meanwhile, the train speed range was 50 km/h to 600 km/h, and although the current speed is less than 350 km/h, the calculation range was made larger to meet the future development needs. The dynamic coefficient curves of a bridge with various vertical natural frequencies are shown in Fig. 10 for a speed range of analysis of every 10 km/h, both with and without taking into account the randomness of material properties. It can be seen that under the deterministic analysis, the train running speed that makes the dynamic coefficient of SSB with vertical natural frequency of 5.13 Hz reach the maximum peak is 460 km/h, respectively. According to Eq. (38), and at this time, the excitation frequency of the train is 5.11 Hz, which is close to the natural vibration frequency of the bridge. The first three order super-harmonic resonance speeds while the train is running and the corresponding order super-harmonic resonance speed in Fig. 10 are compared, as shown in Table 11. The comparison results show that the simulation results are highly consistent with the theoretical analysis results. Furthermore, the dynamic coefficient of the girder body at the second and higher order super-harmonic resonance velocity is much smaller than that of resonance. In addition, the dynamic coefficient of the girder body considering the uncertainty of structural parameters is more than 1.1 times larger than the result of the deterministic calculation, and the train running speed which causes girder body resonance also decreases to a certain extent. The dynamic coefficients of SSBs with natural frequencies of 6.00 Hz and 7.51 Hz show the same change law as the speed of the train changes.

### 4.3 Resonance analysis

#### 4.3.1 Influence of natural frequency of bridge and train speed on resonance characteristics

The natural frequency of the SSB is expressed by Eq. (40).

$$f_b = \frac{m}{L_b} \tag{40}$$

where $m$ is the fundamental frequency coefficient and $L_b$ is the SSB′s span.

By modifying the section form of a simply supported bridge, the natural frequency can be altered while the design weight of a HSR bridge is fixed. The relationship between bending stiffness and the vertical natural frequency of the SSB is depicted in Fig. 11. The increase in bending stiffness leads to an improvement in the

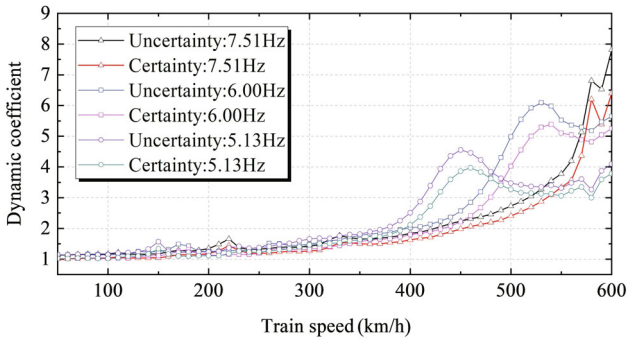


**Fig. 10 Dynamic coefficients under deterministic and uncertain analysis**

**Table 10 CRH2 model parameters**

| Parameters | Symbol | Unit | Motor car | Trail car |
|---|---|---|---|---|
| Car body mass | $m_c$ | kg | $2.88\times10^4$ | $2.88\times10^4$ |
| Bogie mass | $m_t$ | kg | $2.6\times10^3$ | $2.6\times10^3$ |
| Wheel mass | $m_w$ | kg | $1.97\times10^3$ | $1.97\times10^3$ |
| Moment of inertia of car body | $J_c$ | kg·m$^2$ | $1.441\times10^6$ | $1.441\times10^6$ |
| Bogie moment of inertia | $J_t$ | kg·m$^2$ | $1.424\times10^3$ | $1.424\times10^3$ |
| Half wheelbase | $L_t$ | m | 1.25 | 1.25 |
| Bogie half distance | $L_c$ | m | 8.75 | 8.75 |
| Primary suspension stiffness | $k_p$ | N/m | $1.176\times10^6$ | $1.176\times10^6$ |
| Secondary suspension stiffness | $k_s$ | N/m | $1.764\times10^5$ | $1.764\times10^5$ |
| Primary suspension damping | $c_p$ | N·s/m | $1.96\times10^4$ | $1.96\times10^4$ |
| Secondary suspension damping | $c_s$ | N·s/m | $9.8\times10^3$ | $9.8\times10^3$ |

bridge′s vertical natural frequency. Additionally, for a given bending stiffness, the natural frequency decreases with increasing span size.

To further explore the influence of the bridge′s natural frequency and train′s running speed on the dynamic characteristics of the SSB, dynamic coefficients corresponding to different bridge vertical natural frequency are calculated when the CRH2 train passes through 24 m, 32 m and 40 m span SSB at different speeds, and the resulting curves are shown in Fig. 12. Several conclusions can be observed: (a) when the natural frequency is not in the resonance region, the dynamic coefficient corresponding to the same vertical natural frequency increases with the improvement of the speed of the train; (b) the higher the train speed, the higher the vertical natural frequency and dynamic coefficient of the girder when resonance occurs. Therefore, increasing the bridge′s vertical natural frequency can effectively improve the resonance speed and reduce the dynamic coefficient of the train traveling at a fixed speed; (c) when the train with a fixed speed causes the resonance of the simply supported bridge, the vertical natural frequency improves with the increase of the span, while the dynamic coefficient diminishes with the improvement of the span; and (d) when the train′s speed is constant, the dynamic coefficient of the girder with $n$-order super-harmonic resonance does not necessarily decrease with the increase of order, but it is far less than that of resonance.

#### 4.3.2 Research on natural frequency limit of SSB at design speed of 400 km/h

Figure 13 gives the maximum dynamic coefficient $\beta_{\max}$ curve of the girder body under different vertical vibration frequencies within the range of 200 km/h–400 km/h. According to Table 9, the allowable dynamic coefficients of the CRH2 train running on 24 m, 32 m and 40 m span simply supported bridges are 3.26, 3.53 and 3.65, respectively. It can be seen that with the increase of vertical natural frequency, the maximum dynamic response curve of the SSB has experienced three stages:

(1) On the left side of the sensitive range: when the resonance velocity of the bridge is $v_{v,1}=3.6d_v f_b<400$ km/h, the bridge will resonate in the design speed, and the maximum dynamic coefficient of the simply supported bridge changes slightly and increases slowly with the increase of the vertical natural frequency.

(2) In the sensitive range: when the resonance velocity of the bridge is $v_{v,1}=3.6d_v f_b$, it is close to 400 km/h, and the peak value of the SSB′s response is directly related to the vertical natural frequency. In this range, increasing the vertical natural frequency can effectively reduce the maximum dynamic coefficient.

(3) On the right side of the sensitive range, when the resonance velocity is $v_{v,1}=3.6d_v f_b>400$ km/h, the bridge will not resonate in the design speed. The SSB′s dynamic response is small, and almost no longer affected by the vertical natural frequency.

When the train′s maximum design speed is 400 km/h, the vertical natural frequency of the 24 m span SSB enters the sensitive range at about 110/$L$ Hz, and the peak value of the maximum dynamic coefficient is about 7.78. The maximum dynamic coefficient is about 150/$L$ Hz when the vertical vibration frequency of the bridge exceeds the sensitive range, and the maximum dynamic coefficient of the girder is less than 2.38. The sensitive range of vertical

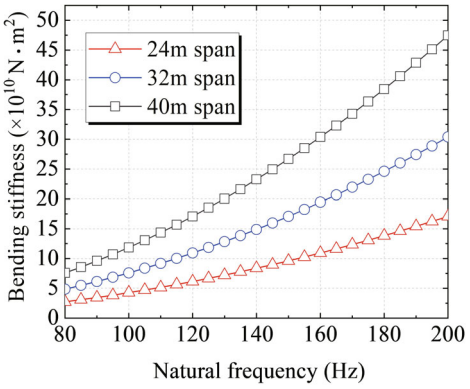


**Fig. 11 Relationship between bending stiffness and natural frequency**

**Table 11 Super-harmonic resonance parameters of bridge with natural frequency of 5.13 Hz**

| Order of super- harmonic resonance | 1 | 2 | 3 |
|---|---|---|---|
| Theoretical speed (km/h) | 461.7 | 230.9 | 153.9 |
| Uncertainty speed (km/h) | 450 | 230 | 150 |
| Certainty speed (km/h) | 460 | 230 | 150 |
| Uncertainty dynamic coefficient | 4.55 | 1.42 | 1.57 |
| Certainty dynamic coefficient | 3.97 | 1.26 | 1.34 |
| $\varepsilon_1$ | 0.975 | 0.996 | 0.975 |
| $\varepsilon_2$ | 0.996 | 0.996 | 0.975 |
| $\zeta$ | 1.15 | 1.13 | 1.17 |

Note: $\varepsilon_1$ and $\varepsilon_2$ represent the ratio of the results of uncertainty analysis and certainty analysis to the theoretical velocity results respectively, and $\zeta$ represents the ratio of the dynamic coefficients of uncertainty analysis and certainty analysis.

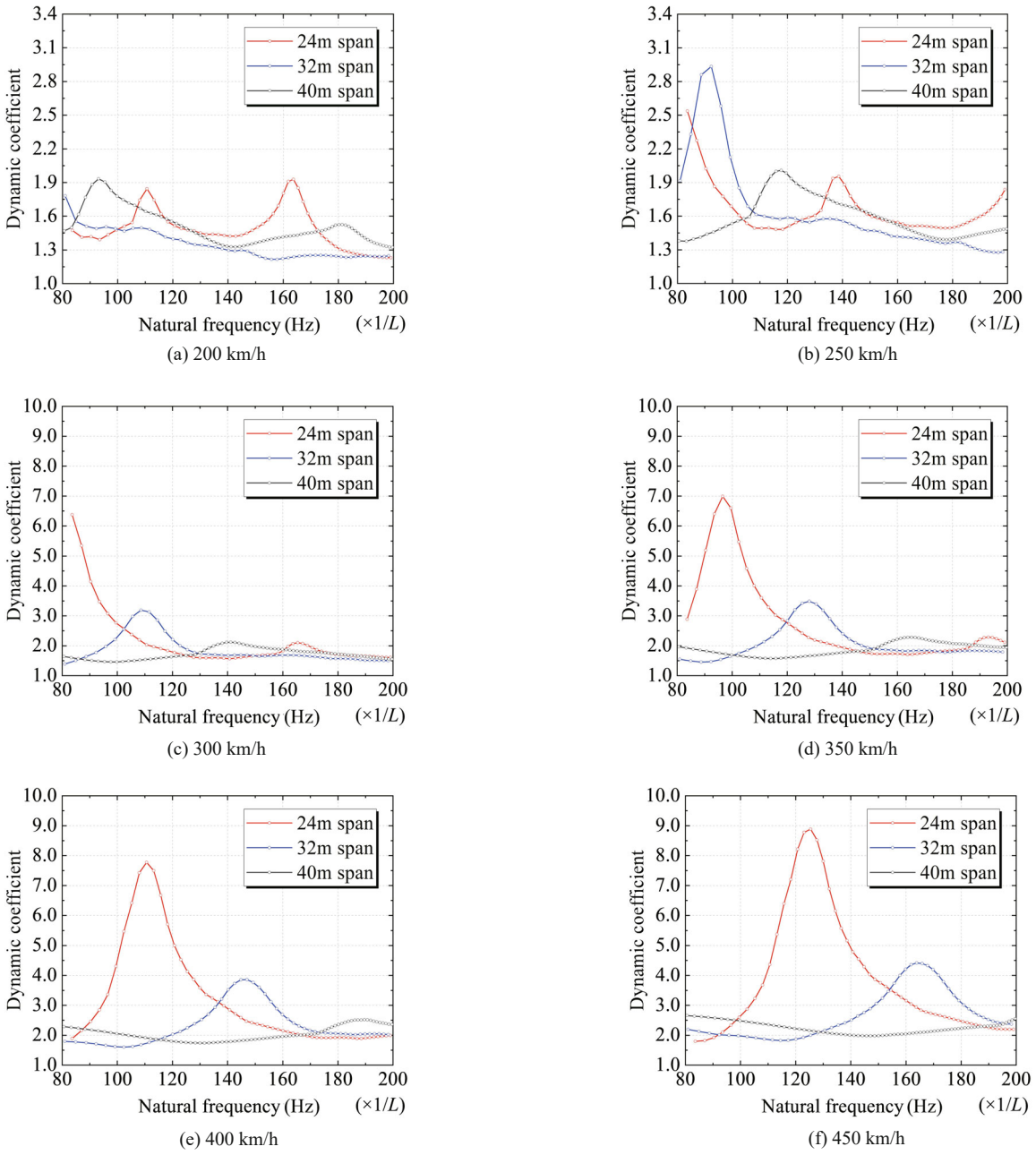


**Fig. 12 Dynamic coefficients of beams with different vertical natural frequencies**

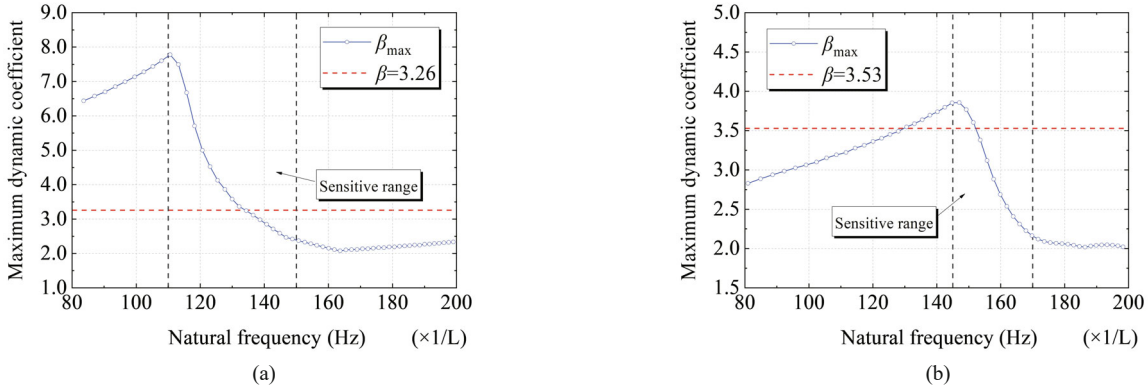


**Fig. 13 Maximum dynamic coefficient of beam under different natural frequencies: (a) 24 m; (b) 32 m**

**Table 12 Lower limit values of bridge natural frequency in different specifications (Data from Zhai and Xia (2012))**

| Source | 24 m span | 32 m span | 40 m span |
|---|---|---|---|
| EUROCODE | 3.63 Hz | 3.07 Hz | 2.69 Hz |
| Chinese Code | 5.00 Hz | 3.75 Hz | 3.00 Hz |
| Japanese Code | 6.29 Hz | 5.00 Hz | 4.18 Hz |
| Proposed | 6.25 Hz | 5.00 Hz | 3.00 Hz |

natural frequency of the 32 m span simply supported bridge is about 145/$L$ Hz–170/$L$ Hz. The peak value of the maximum dynamic coefficient in the sensitive area is about 3.86, and the maximum dynamic coefficient is stable below 2.12 beyond the sensitive area.

For the 40 m span simply supported bridge, because the dynamic coefficient under different train running speeds is far less than the allowable value 3.65, its safety can be guaranteed in the common range of the vertical natural frequency; therefore, the lower limit of natural frequency of this span bridge can be appropriately relaxed, and 3 Hz in the Chinese code is recommended.

In summary, when the design speed of train is 400 km/h, the lower limit of vertical natural frequencies of the 24 m and 32 m span simply supported concrete bridges of HSR is 150/$L$ (6.25 Hz) and 160/$L$ (5.00 Hz), which can effectively reduce the dynamic response of simply supported concrete bridges. A comparison between the results obtained and those in different specifications is shown in Table 12. Since there is no requirement of more than 400 km/h in the current specification, the comparison is only for trains with speeds of 350 km/h and below. It can be found that the lower limit value calculated in this study is close to the Japanese Code and greater than the current Chinese specification and European specifications, indicating that the existing natural frequency limit value in the specification is not applicable to the operation of 400 km/h speed-up trains, and should be adjusted accordingly.

## 5 Conclusions

To analyze the natural frequency limit of HSR bridges, a coupled vibration model of the train-bridge considering the material parameters random field is established. The train model is established by a mass-spring-damping system and the SSB is modeled by the SFEM method. The elastic modulus, density and other structural parameters of the bridge are set as random fields following a Gaussian process, which are discretized by KLE. Based on the SFEM, the corresponding stiffness, mass and damping matrices are constructed, and the Newmark-$\beta$ method is adopted to resolve the dynamic model. Then the statistical moment of the response data of the train and the bridge are output by PEM. There are several main conclusions:

(1) KLE-PEM-3 can accurately calculate the SFEM dynamic problems, and the computational efficiency is more than two orders of magnitude higher than the traditional MCS.

(2) Considering the uncertainty analysis of the spatial random field of structural parameters, the dynamic response of a simply supported bridge is more than 12% larger than that of a deterministic analysis, and the train running speed decreases to a certain extent when the bridge resonates.

(3) The dynamic response caused by resonance can be effectively prevented by avoiding the bridge′s vertical frequency from getting close to the excitation frequency of the train, and the improvement of the vertical vibration frequency of the HSR bridge can effectively improve the resonance speed and diminish the dynamic coefficient of the train running at a certain speed.

(4) When the design speed of the train is 400 km/h, the dynamic response of the SSB can be effectively reduced by limiting 150/$L$ (6.25 Hz) and 160/$L$ (5.00 Hz) under the vertical natural vibration frequency of SSB with span of 24 m and 32 m. The lower limit value is not required for SSB with a span of 40 m.

## Acknowledgement

The work described in this study is supported by grants from the Open Fund of Hunan International Scientific and Technological Innovation Cooperation Base of Advanced Construction and Maintenance Technology of Highway (Changsha University of Science and Technology) Project Number kfj210803, National Natural Science Foundation of China (Grant Nos. U1934207 and 11972379) and Fujian University of Technology (GY-Z21181).

## References

Çavdar Ö, Bayraktar A and Adanur S (2010), "Stochastic Finite Element Analysis of a Cable-Stayed Bridge System with Varying Material Properties," *Probabilistic Engineering Mechanics*, **25**(2): 279–289.

Chang T (2014), "Stochastic Dynamic Finite Element Analysis of Bridge–Vehicle System Subjected to Random Material Properties and Loadings," *Applied Mathematics and Computation*, **242**: 20–35.

Chen Z and Zhai W (2019), "Theoretical Method of Determining Pier Settlement Limit Value for China′s High-Speed Railway Bridges Considering Complete Factors," *Engineering Structures*, **209**: 109998.

Chen Z, Zhai W and Tian G (2018), "Study on the Safe Value of Multi-Pier Settlement for Simply Supported Girder Bridges in High-Speed Railways," *Structure and Infrastructure Engineering*, **14**(1–3): 400–410.

Ghanem R and Spanos P (2003), *Stochastic Finite Elements: A Spectral Approach*, Courier Corporation, USA.

Gharad AM and Sonparote RS (2021), "Evaluation of Vertical Impact Factor Coefficients for Continuous and Integral Railway Bridges Under High-Speed Moving Loads," *Earthquake Engineering and Engineering Vibration*, **20**(2): 495–504. https://doi.org/10.1007/s11803-021-2034-7

Jiang L, Liu X, Xiang P and Zhou W (2019), "Train-Bridge System Dynamics Analysis with Uncertain Parameters Based on New Point Estimate Method," *Engineering Structures*, **199**: 109454.

Jin Z, Pei S, Li X and Qiang S (2015), "Probabilistic Evaluation Approach for Nonlinear Vehicle–Bridge Dynamic Performances," *Journal of Sound and Vibration*, **339**: 143–156.

Jin Z, Yuan L and Pei S (2020), "Efficient Evaluation of Bridge Deformation for Running Safety of Railway Vehicles Using Simplified Models," *Advances in Structural Engineering*, **23**(3): 454–467.

Lai Z, Jiang L, Liu X, Zhang Y and Zhou W (2021), "Analytical Investigation on the Geometry of Longitudinal Continuous Track in High-Speed Rail Corresponding to Lateral Bridge Deformation," *Construction and Building Materials*, **268**: 121064.

Liu X, Jiang L, Lai Z, Xiang P and Chen Y (2020a), "Sensitivity and Dynamic Analysis of Train-Bridge Coupled System with Multiple Random Factors," *Engineering Structures*, **221**: 111083.

Liu X, Jiang L, Xiang P, Lai Z, Feng Y and Cao S (2021a), "Dynamic Response Limit of High-Speed Railway Bridge Under Earthquake Considering Running Safety Performance of Train," *Journal of Central South University*, **28**: 968–980.

Liu X, Jiang L, Xiang P, Lai Z, Liu L, Cao S and Zhou W (2021b), "Probability Analysis of Train-bridge Coupled System Considering Track Irregularities and Parameter Uncertainty," *Mechanics Based Design of Structures and Machines*, **51**(5): 2918–2935.

Liu X, Jiang L, Xiang P, Lai Z, Zhang Y and Liu L (2022), "A Stochastic Finite Element Method for Dynamic Analysis of Bridge Structures Under Moving Loads," *Structural Engineering and Mechanics*, **82**(1): 31–40.

Liu X, Xiang P, Jiang L, Lai Z, Zhou T and Chen Y (2020b), "Stochastic Analysis of Train-Bridge System Using the Karhunen-Loeve Expansion and the Point Estimate Method," *International Journal of Structural Stability and Dynamics*, **20**(2): 2050025.

Montenegro P, Calçada R, Vila N and Tanabe M (2016), "Running Safety Assessment of Trains Moving over Bridges Subjected to Moderate Earthquakes: Running Safety of Trains Moving over Bridges Subjected to Earthquakes," *Earthquake Engineering and Structural Dynamics*, **45**(3): 483–504.

Montenegro P, Carvalho H, Ribeiro D, Calçada R, Tokunaga M, Tanabe M and Zhai W (2021), "Assessment of Train Running Safety on Bridges: A Literature Review," *Engineering Structures*, **241**: 112425.

Perrin G, Soize C, Duhamel D and Funfschilling C (2013), "Track Irregularities Stochastic Modeling," *Probabilistic Engineering Mechanics*, **34**: 123–130.

Rahman S and Xu H (2004), "A Univariate Dimension-Reduction Method for Multi-Dimensional Integration in Stochastic Mechanics," *Probabilistic Engineering Mechanics*, **19**(4): 393–408.

Rocha J, Henriques A and Calçada R (2012), "Safety Assessment of a Short Span Railway Bridge for High-Speed Traffic Using Simulation Techniques," *Engineering Structures*, **40**: 141–154.

Rocha J, Henriques A and Calçada R (2016), "Probabilistic Assessment of the Train Running Safety on a Short-Span High-Speed Railway Bridge," *Structure and Infrastructure Engineering*, **12**(1): 78–92.

Siringoringo D and Fujino Y (2012), "Estimating Bridge Fundamental Frequency from Vibration Response of Instrumented Passing Vehicle: Analytical and Experimental Study," *Advances in Structural Engineering*, **15**: 417–433.

Sofi A and Romeo E (2018), "A Unified Response Surface Framework for the Interval and Stochastic Finite Element Analysis of Structures with Uncertain Parameters," *Probabilistic Engineering Mechanics*, **54**: 25–36.

Wu S and Law S (2010), "Dynamic Analysis of Bridge–Vehicle System with Uncertainties Based on the Finite Element Model," *Probabilistic Engineering Mechanics*, **25**(4): 425–432.

Xin L, Li X, Zhang J, Zhu Y and Xiao L (2020), "Resonance Analysis of Train–Track–Bridge Interaction Systems with Correlated Uncertainties," *International Journal of Structural Stability and Dynamics*, **20**(1): 2050008.

Xin L, Li X, Zhu Y and Liu M (2019), "Uncertainty and Sensitivity Analysis for Train-Ballasted Track–Bridge System," *Vehicle System Dynamics*, **58**: 1–19.

Xu L, Li Z, Zhao Y, Yu Z and Wang K (2020), "Modelling of Vehicle-Track Related Dynamics: A Development of Multi-Finite-Element Coupling Method and Multi-Time-Step Solution Method," *Vehicle System Dynamics*, **60**(4): 1097–1124.

Xu L, Zhai W and Gao J (2017), "A Probabilistic Model for Track Random Irregularities in Vehicle/Track Coupled Dynamics," *Applied Mathematical Modelling*, **51**: 145–158.

Xu L, Zhai W and Li Z (2018), "A Coupled Model for Train-Track-Bridge Stochastic Analysis with Consideration of Spatial Variation and Temporal Evolution," *Applied Mathematical Modelling*, **63**: 709–731.

Yang Y and Wu Y (2002), "Dynamic Stability of Trains Moving over Bridges Shaken by Earthquakes," *Journal of Sound and Vibration*, **258**(1): 65–94.

Yang Y, Yao Z and Wu Y (2004), *Vehicle-Bridge Interaction Dynamics: With Applications to High-Speed Railways*, River Edge, NJ: World Scientific, USA.

Yang Y and Yau J (2015), "Vertical and Pitching Resonance of Train Cars Moving over a Series of Simple Beams," *Journal of Sound and Vibration*, **337**: 135–149.

Yang Y and Yau J (2017), "Resonance of High-Speed Trains Moving over a Series of Simple or Continuous Beams with Non-Ballasted Tracks," *Engineering Structures*, **143**: 295–305.

Yang Y, Yau J and Hsu L (1997), "Vibration of Simple Beams Due to Trains Moving at High Speeds," *Engineering Structures*, **19**(11): 936–944.

Yang Y, Yau J and Urushadze S (2019), "Wave Transmission of Linked Railcars Moving over Multi Simple Beams Under Dual Resonance," *Journal of Sound and Vibration*, **452**: 51–57.

Zeng Q, Yang Y and Dimitrakopoulos E (2016), "Dynamic Response of High Speed Vehicles and Sustaining Curved Bridges Under Conditions of Resonance," *Engineering Structures*, **114**: 61–74.

Zhai W and Xia H (2012), *Train-Track-Bridge Dynamic Interaction: Theory and Engineering Application*, Beijing: Science Press, China.

Zhao Y and Ono T (2000), "New Point Estimates for Probability Moments," *Journal of Engineering Mechanics*, **126**(4): 433–436.